J Solid State Electrochem (2007) 11:1671–1677
DOI 10.1007/s10008-007-0325-1

ORIGINAL PAPER

Synthesis and characterization of $LiCo_xMn_{2-x}O_4$ powder by a novel CAM microwave-assisted sol–gel method for Li ion battery

K. Suryakala · K. R. Marikkannu · G. Paruthimal Kalaignan · T. Vasudevan

Received: 27 December 2006 / Revised: 15 March 2007 / Accepted: 4 April 2007 / Published online: 4 May 2007

Abstract $LiMn_2O_4$-based spinels are of great interest as positive electrode materials for lithium ion batteries. $LiCo_xMn_{2-x}O_4$ (x=0.0, 0.1, 0.2, 0.3, and 0.4) spinel phases have been synthesized by novel citric acid-modified microwave-assisted sol–gel method. The structural properties of the synthesized products have been investigated by X-ray powder diffraction and scanning electron microscopy. To improve the recharge capacity of $Li/LiCo_xMn_{2-x}O_4$ cells, the electrochemical features of $LiCo_xMn_{2-x}O_4$ compounds have been evaluated as positive electrode materials. The structural properties of Co-doped oxides are very similar to $LiMn_2O_4$ electrode. Techniques like cyclic voltammetry, charge–discharge and cycle life are also used to characterize the $LiCo_xMn_{2-x}O_4$ (x=0.0, 0.1, 0.2, 0.3, and 0.4) electrodes.

Keywords Citric acid-modified (CAM) microwave-assisted sol–gel method · Lithium manganese oxide · Co-doped lithium manganate · Cubic spinel compound · Efficiency · Cyclic voltammetry · Lithium ion battery

Introduction

Secondary lithium batteries have been studied for the past several decades, as they exhibit the highest specific energy. Since the introduction of the rechargeable lithium ion battery by Sony Energy Technical in 1990 [1], much research effort has been made to develop lithium ion battery cathode materials to meet the demands of the market. Among the cathode materials (such as $LiCoO_2$, $LiNiO_2$, $LiCo_{1-x}Ni_{1-x}O_2$, and $LiMn_2O_4$), the Li–Mn spinel is one of the most promising candidates in terms of its low cost, easy preparation, and non-toxicity. However, the loss in capacity is remarkable upon cycling, which is believed to be mainly a result of the Jahn–Teller effect and a slow dissolution of the $LiMn_2O_4$ electrode into the electrolyte. The numerous works have been done to improve the performances, including preparing Li–Mn spinel with small specific surface, partially substituted by some of the transition metals, such as Co [2], Ni [3], Fe [4], Cr [5], Zn [6], Cu [7], etc., to enhance structural stability. The electrochemical behavior of these materials also depends on the method of synthesis.

Therefore, to overcome these disadvantages, various new techniques have been developed. Such techniques are based on the processes of co-precipitation, ion exchange, or thermal decomposition at low temperatures of appropriate organic precursors obtained by sol–gel [8], Pechini process [9], freeze-drying [10], melt-impregnation [11], or citric acid gel [12] methods. These methods lead to homogeneous spinel materials with small particle size at the low cost of expensive reagents and process complexity.

In this work, an attempt has been made to stabilize the $LiMn_2O_4$ spinel structure by a citric acid-modified (CAM) microwave-assisted sol–gel method that employs citric acid as a chelating agent and acryl amide as a gelling agent with Co as dopant. This soft chemistry technique offers many advantages such as better homogeneity and regular morphology of products, low calcination temperature, shorter heating time, sub-micron-sized particles, less impurities, large surface area, and good control of stoichiometry.

K. Suryakala · K. R. Marikkannu ·
G. Paruthimal Kalaignan (✉) · T. Vasudevan
Lithium Battery Research Laboratory,
Department of Industrial Chemistry, Alagappa University,
Karaikudi, Tamil Nadu 630 003, India
e-mail: kalaignan@yahoo.com

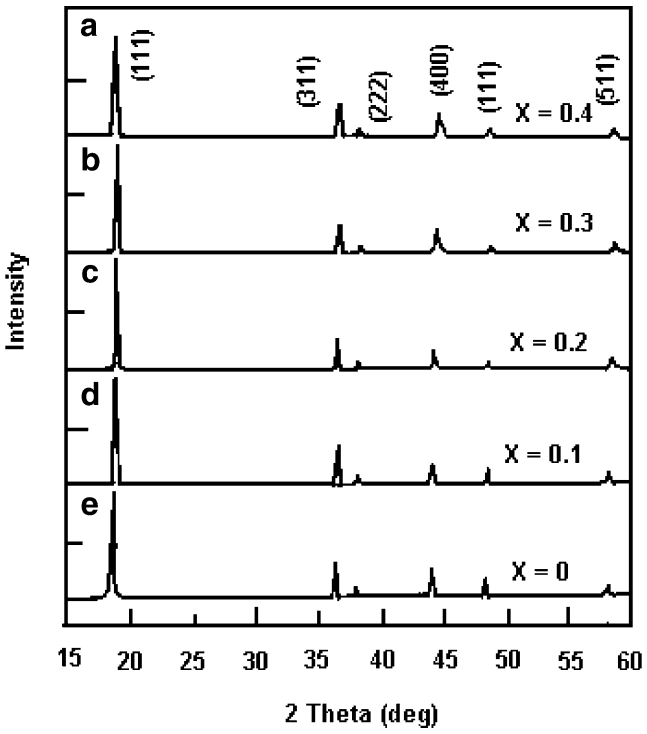

Fig. 1 XRD pattern of $LiCo_xMn_{2-x}O_4$. *a* x=0.0, *b* x=0.1, *c* x=0.2, *d* x=0.3, and *e* x=0.4

Experimental

Synthesis procedure

All the chemical reagents used in the experiments were analytical grade without further purification. $LiCo_xMn_{2-x}O_4$ powders were synthesized by CAM microwave-assisted sol–gel method. A stoichiometric amount of lithium nitrate, manganese acetate, and cobalt-(II) nitrate were dissolved in triple distilled water. A calculated amount of citric acid was added as a complexing agent followed by the addition of acryl amide. Here, the acryl amide acts as a gelling agent. The resulting solution was mixed with continuous magnetic stirring at 90 °C until a clear viscous gel occurs. The obtained precursor was preserved under vacuum at 100 °C for 12 h to eliminate water adequately and then was placed in microwave oven. The microwave power operated at 100% (650 W) for 20 min. After the microwave treatment, the samples were calcined at 550 °C for 6 h, followed by slowly cooling to room temperature.

Physical characterization

X-ray diffraction studies

The purity and structural conformity of the powder was confirmed by JEOL X-ray diffraction analysis (JDX-8030) using Cu Kα radiation. The diffraction patterns were obtained at 25 °C in the range $10° \geq 2\theta \leq 60°$. The step size and scan rate were set at 0.1 and 2 °C min^{-1}, respectively.

SEM analysis

To investigate the particle nature and size of the product, scanning electron micrograph (SEM) was taken with a JEOL scanning electron microscope (JSM-840A).

Electrochemical characterization

Cyclic voltammetry was performed in the potential window of 2.5–4.5 V in 1 M $LiClO_4$ in ethylene carbonate (EC)/propylene carbonate (PC; 1:1 *v*/*v*) as the electrolyte. $LiClO_4$ salt was kept for 24 h in an oven at 120 °C to eliminate the water molecules, followed by immersion in 4 Å molecular sieves (sodium aluminum silicate) to absorb the extra moisture. Polypropylene sheet was used as the separator, which was chocked in 1 M $LiClO_4$/EC/PC (1:1) electrolyte. The cells were assembled in an argon-filled glove box. The humidity and oxygen content inside the box were maintained at ppm levels.

To assess the cycling behavior of the synthesized cathode materials, cyclic voltammetry and charge/discharge studies were conducted by fabricating 2,016 button-type electrochemical cells with the configuration of $C/LiCo_xMn_{2-x}O_4$ and employing Li^+ ion conducting, $LiClO_4$ electrolyte. The cathode was prepared by mixing synthesized powders, acetylene black, and a polyvinylidene difluoride (PVDF) binder dissolved with 2-NMP in an 80:10:10 weight ratio. The above composite material was mixed and was placed in a die and pressed into an expanded aluminum foil at a pressure of 5 tonnes cm^{-2} using a hydraulic press to yield circular pellet electrodes. The pellets were then dried at 110 °C in an air oven. Cyclic voltammograms were recorded at a slow scan rate of 1 mV/s over the potential range of 2.5–4.5 V using an EG&G electrochemical analyzer. The synthesized cathode electrodes were examined for their capacity by constant current charge/discharge at potential window 3.0–4.5 V at a constant current density of 0.1 mA/cm^2 using WonATech potentiostat/galvanostat instrument (WPG100 South Korea).

Table 1 Unit cell parameters 'a' of $LiCo_xMn_{2-x}O_4$

Composition	'a' (Å)
$LiMn_2O_4$	8.242
$LiCo_{0.1}Mn_{1.9}O_4$	8.234
$LiCo_{0.2}Mn_{1.8}O_4$	8.218
$LiCo_{0.3}Mn_{1.7}O_4$	8.200
$LiCo_{0.4}Mn_{1.6}O_4$	8.173

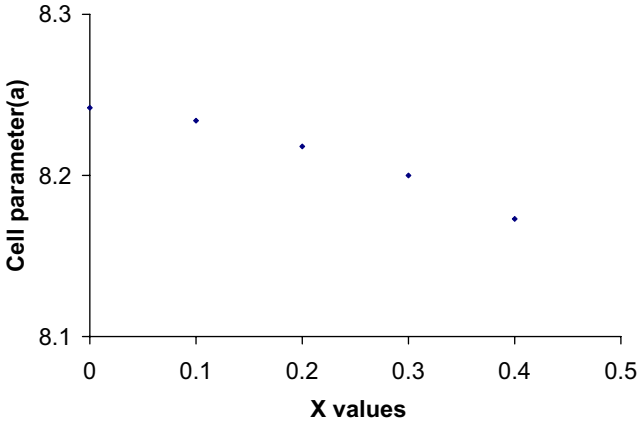

Fig. 2 Unit cell parameter of $LiCo_xMn_{2-x}O_4$ (x=0.0–0.4)

Results and discussion

Phase formation results X-ray diffraction

The powder X-ray diffraction (XRD) patterns of $LiCo_xMn_{2-x}O_4$ (x=0.0–0.4) are shown in Fig. 1. The $LiCo_xMn_{2-x}O_4$ samples have a single-phase spinel structure. This indicates that the Co^{3+} ions substitute the Mn sites homogeneously, while retaining the Fd3m space group. The peaks in each XRD pattern can be indexed on the basis of a cubic unit cell. The ideal crystal structure of $LiCo_xMn_{2-x}O_4$ with a cubic cell contains 56 atoms, 8 Li, 16 Mn (Co), and 32 (O). The crystal structure can be described as Mn (Co) ions occupying one half of the octahedral sites (16d) and Li ions present on eight of the tetrahedral sites (8a) and within the cubic close-packed oxide array [13]. The structure refinement was carried out by the Rietveld method [14]. The unit cell parameter of the $LiCo_xMn_{2-x}O_4$ (x=0.0–0.4) composition is indicated in Table 1. The variation in lattice parameter as a function of x values for $LiCo_xMn_{2-x}O_4$ powders, synthesized by CAM microwave-assisted sol gel method, is shown in Fig. 2. The observed and calculated

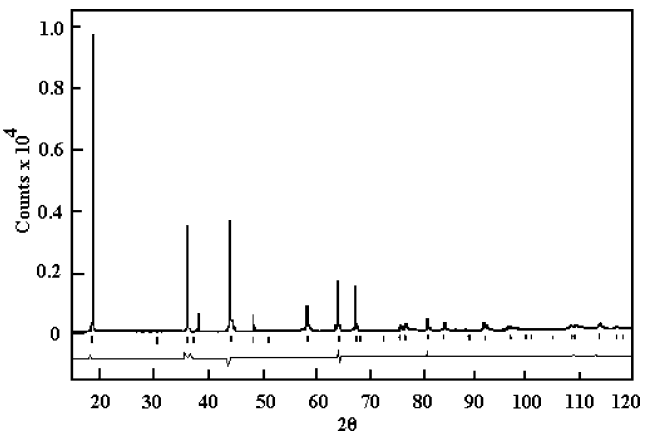

Fig. 3 XRD profile of $LiCo_{0.3}Mn_{1.7}O_4$

Table 2 Particle properties of $LiCo_xMn_{2-x}O_4$ (x=0.0–0.4)

Sample	Specific surface area (m^2/g)	Crystalline size (nm)
$LiMn_2O_4$	8.4	33
$LiCo_{0.1}Mn_{1.9}O_4$	8.6	31
$LiCo_{0.2}Mn_{1.8}O_4$	8.7	32
$LiCo_{0.3}Mn_{1.7}O_4$	8.9	33
$LiCo_{0.4}Mn_{1.6}O_4$	8.9	33

XRD profiles of the sample with x=0.3 are shown in Fig. 3 (Rietveld method). The resultant XRD values obtained are similar to that of earlier literature [15].

Although the Mn ions in the solid solution are located in the octahedral sites, Co coexists with Mn in these sites. This causes the Mn–O bond lengths to depend not only on the valence state of Mn but also on the concentration and valence state of Co. The lattice constant 'a' and the cell volume decreases with the addition of Co, as shown in Fig. 2. This is due to the smaller size of the substituting Co^{3+} ion (0.545 Å for the coordination number 6, in low crystal field) as compared with the larger Mn^{3+} ion (0.645 Å) for coordination number 6, in low crystal field [16]. If however, Co^{3+} substitutes into the Mn^{4+} site 0.53 Å for coordination number 6 in low crystal field [17], an increase in the lattice constant 'a' with increasing x in $LiCo_xMn_{2-x}$ O_4 can be found. Therefore, based on our results, it is concluded that Co^{3+} substitutes into the Mn^{3+} sites. The Co ion has a large binding energy (1,067 KJ mol^{-1} in CoO_6 than the Mn ions in MnO_6 octahedra 946 KJ mol^{-1}) [18], so that the Co ion prefers to substitute at the octahedral Mn site and substitutes for the Mn^{3+} ion. The formula can be written in the form of $LiMn_{1-x}^{4+}$ Mn_{1-x}^{3+} $Co_x^{3+}O_4$ [19].

The intensity ratio I_{311}/I_{400} is considered to be sensitive to the cation distribution that depends upon the amount of substitution. It is observed that the relative intensity decreases linearly with decrease of Co substitution or increase of Mn content. The diffraction data proved that the synthesized samples have been formed with cubic spinel structure. The crystalline size and specific surface area of $LiCo_xMn_{2-x}O_4$ powders are summarized in Table 2. The crystalline size was calculated from the XRD pattern by using Scherrer's equation. Calculation was done by using the XRD peak of the crystallite plane .The crystallite size for all samples prepared in this work was approximately 30 nm. The specific surface area for all the samples was measured by Brunauer–Emmett–Teller (BET) method. The specific surface area of $LiCo_xMn_{2-x}O_4$ powders range from 5 to 12 m^2/g.

Scanning electron microscopy

SEM observations of the synthesized samples are shown in Fig. 4a–e. The micrograph shows that all samples have

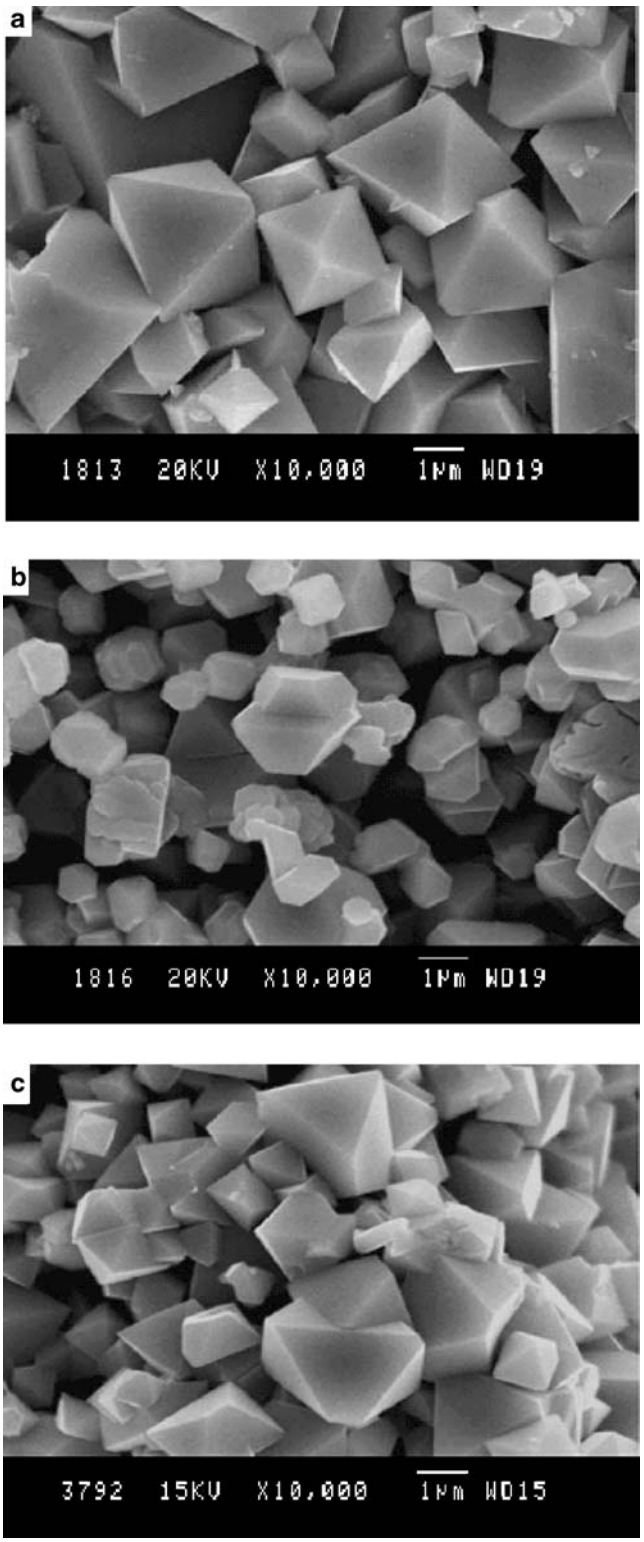

Fig. 4 Scanning electron micrograph of $LiCo_xMn_{2-x}O_4$. **a** x=0.0, **b** x=0.1, **c** x=0.2, **d** x=0.3, and **e** x=0.4

regular shapes with well-defined crystal faces. The undoped material has exhibited bigger and uniform size particles (Fig. 4a). Figure 4b shows the Co-doped $LiMn_2O_4$. In this figure, the shape of the particles

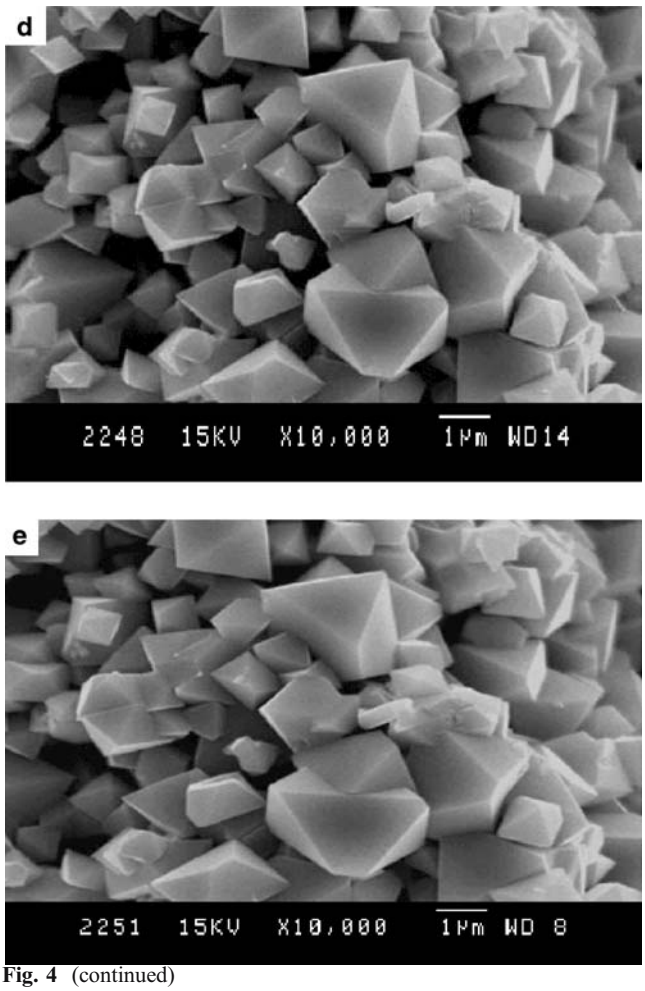

Fig. 4 (continued)

distributed on the surface was changed from regular to irregular. This indicates the presence of Co particles in $LiMn_2O_4$. As the concentration of Co increases, the amount of irregular particles also increased. Based on the

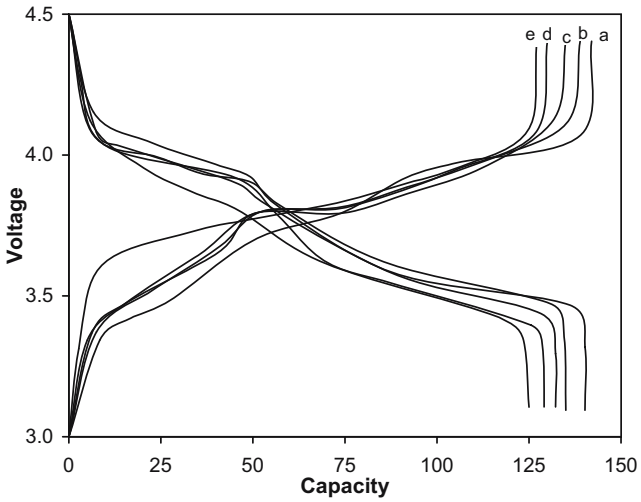

Fig. 5 Charge–discharge behavior of $LiCo_xMn_{2-x}O_4$. **a** x=0.0, **b** x=0.1, **c** x=0.2, **d** x=0.3, and **e** x=0.4

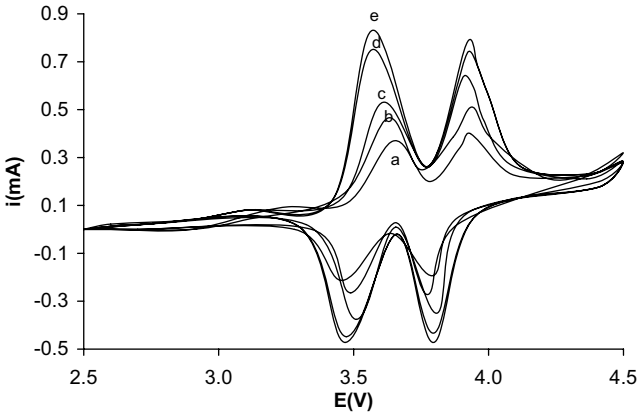

Fig. 6 Cyclic voltammogram of $LiCo_xMn_{2-x}O_4$. **a** x=0.0, **b** x=0.1, **c** x=0.2, **d** x=0.3, and **e** x=0.4

results, the intercalation of Co particles in $LiMn_2O_4$ was clearly confirmed (Fig. 4c–e). The average particle size of the Co-doped spinel crystallites is 1–4 μm. The narrow particle size distribution of as prepared samples is important for good electrochemical properties.

Charge–discharge studies

Figure 5a–e shows the first charge/discharge curves of Li/$LiCo_xMn_{2-x}O_4$ (0.0–0.4) cells. It can be seen obviously that the charge/discharge curves of all the samples has twovoltage plateaus at approximately 3.5 and 4.5 V, which indicated a remarkable characteristic of a well-defined $LiMn_2O_4$ spinel. The two voltage plateaus indicate that the insertion and extraction of lithium ions occur in two stages [4, 20]. The first stage, voltage plateau at about 3.5 V, is attributed to the removal of lithium ions from half of the tetrahedral sites in which Li–Li interactions occur. The second stage, voltage plateau observed at 4.1 V, is due to the removal of lithium ions from the other tetrahedral sites in which lithium ions do not have Li–Li interactions. The initial capacity of doped $LiCo_xMn_{2-x}O_4$ (x=0.1–0.4) is lower than that of pure $LiMn_2O_4$. Theoretical capacity of $LiMn_2O_4$ is 148 mAh g^{-1}. From CAM microwave-assisted sol–gel method, the observed capacity of $LiMn_2O_4$ is 142 mAh g^{-1}. The initial capacities of $LiCo_{0.1}Mn_{1.9}O_4$, $LiCo_{0.2}Mn_{1.8}O_4$, $LiCo_{0.3}Mn_{1.7}O_4$, and $LiCo_{0.4}Mn_{1.7}O_4$ are 138.9, 135, 130, and 127.1 mAh g^{-1}, respectively. This decrease of initial capacity is due to decreasing amount of Mn^{3+} ions in Co-substituted spinel phase. In fact, only the Mn^{3+} contributes to charge/discharge capacity during the intercalation–deintercalation of Li^+ in $LiMn_2O_4$.

Cyclic voltammetry studies

Figure 6a–e shows the cyclic voltammogram of $LiMn_2O_4$ and $LiCo_xMn_{2-x}O_4$ (x=0.1–0.4). All voltammograms are carried out at a sweep rate of 1 mV s^{-1}. Two pairs of oxidation and reduction peaks were observed around 3.7 and 4.1 V, and 3.5 and 3.8 V, respectively. The two set of peaks corresponds to the typical two-step reversible intercalation/deintercalation process of lithium ions in $LiCo_xMn_{2-x}O_4$ (x=0.0, 0.1, 0.2, 0.3, and 0.4) spinel. The anodic peaks of cobalt-substituted spinel are taller, sharper, and shifted toward lower potential than that of a pure spinel $LiMn_2O_4$ sample. The anodic peaks shifted toward lower potentials with increase of cobalt substitution, and this suggested that lithium ions need less energy to be removed from the substituted spinels than $LiMn_2O_4$ [21].

The split of the redox peaks into two couples indicates that the electrochemical reactions of the insertion and extraction of lithium ion proceed in two stages [22], which can be written as the following two reactions:

$$(1/2)\,Li^+_+\,(1/2)\,e^- + 2\lambda - MnO_2 \leftrightarrow Li_{0.5}\,Mn_2\,O_4$$

$$(1/2)\,Li^+_+\,(1/2)\,e^- + Li_{0.5}\,Mn_2O_4 \leftrightarrow LiMn_2\,O_4$$

where λ=the defective form of MnO_2.

The addition of cobalt has not affected the electrochemical behavior of $LiMn_2O_4$ because of the appearance of no new peaks.

The first step oxidation peak at about 3.7 V is attributed to the removal of lithium ions from half of the tetrahedral sites in which Li/Li interactions occur. The second step

Table 3 Peak potential differences of $LiCO_xMn_{2-x}O_4$ (x=0.0, 0.1, 0.3, and 0.4)

X in $LiCo_xMn_{2-x}O_4$	Anodic peak potential V vs Li/Li^+		Cathodic peak potential V vs Li/Li^+		Peak potential difference (ΔE_p)	
	I	II	I	II	I	II
0.0	3.72	4.10	3.75	3.50	0.22	0.35
0.1	3.71	4.00	4.70	3.51	0.20	0.30
0.2	3.70	3.95	3.63	3.51	0.19	0.32
0.3	3.63	3.90	3.65	3.53	0.10	0.25
0.4	3.63	4.00	3.70	3.50	0.13	0.30

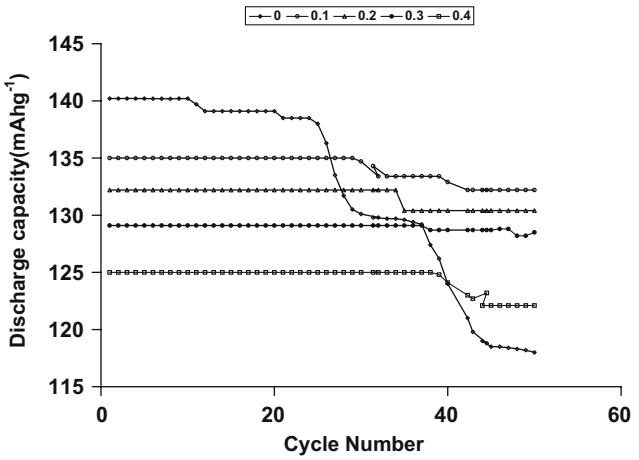

Fig. 7 Cycle life behavior of $LiCo_xMn_{2-x}O_4$ (x=0.0–0.4)

oxidation peak observed at about 4.1 V is due to the removal of lithium ions from the other tetrahedral sites in which lithium ions do not have Li–Li interactions. The peaks show well-defined splitting. This is the characteristic of materials with high degree of crystallinity.

The peak potential separation ΔE_p for the two redox couples will help to study the reversibility of the electrode behavior. Doped $LiMn_2O_4$ electrode that gives minimum ΔE_p value compared to that of the undoped $LiMn_2O_4$ will exhibit maximum reversibility and will be a good battery electrode. Table 3 presents the data derived from typical cyclic voltammograms. All the concentrations of cobalt substitution favor the reversibility for both the redox couples. Particularly, the electrode composition of $LiCo_{0.3}Mn_{1.7}O_4$ gave the very minimum ΔE_p values compared to all other compositions. The cyclic voltammogram clearly indicated that the sample prepared at x=0.3/at 550 °C ($LiCo_{0.3}Mn_{1.7}O_4$) gave the minimum ΔE_p values and maximum reversibility. Hence, $LiCo_{0.3}Mn_{1.7}O_4$ electrode composition is the optimum for preparing good battery electrode for the Li ion battery system.

Cycle life

Figure 7 shows the cycle performance of the $LiCo_xMn_{2-x}O_4$ (x= 0.0–0.4). Comparing with the poor cycle performance that occurred with $LiMn_2O_4$ cathode, the substituted spinel exhibited a remarkable improvement of cycle behavior.

Although the pure $LiMn_2O_4$ had the highest initial discharge capacity, its capacity loss was 0.46 mAh/g of the initial value after 50 cycles between 3.5 and 4.4 V at C/3 charge–discharge rate. However, the capacity loss of $LiCo_{0.1}Mn_{1.9}O_4$, $LiCo_{0.2}Mn_{1.8}O_4$, $LiCo_{0.3}Mn_{1.7}O_4$, and $LiCo_{0.4}Mn_{1.6}O_4$ was only 0.05, 0.03, 0.02, and 0.06 mAh/g of its initial capacity at the 50th cycle. Among all, the sample x=0.3/550 °C has been observed to exhibit relatively less capacity fade (0.02 mAh/g) compared to the cycle life obtained other compositions. The Co-doped spinel showed better cycle performance compared with pure $LiMn_2O_4$.

Because substitution of manganese by Co decreases the unit cell volume and the decrease of Mn^{3+} concentration reduces the Jahn–Teller distortion and also stabilizes the structure integrity of the active, improved electrochemical stability of Co-doped $LiMn_2O_4$ electrode is obtained. The strength of Co–O bond is another reason for the enhanced cyclability of Co-doped $LiMn_2O_4$ electrode because the binding energy of Co–O (1067 KJ/mol) is stronger than that of Mn–O (946 KJ/mol).

Conclusions

Using lithium nitrate, manganese acetate, cobalt nitrate, citric acid, and acryl amide as the starting materials, uniform $LiCo_xMn_{2-x}O_4$ powders have been synthesized successfully by CAM microwave–assisted sol–gel method. The results revealed that the cycle performance of $LiCo_xMn_{2-x}O_4$ cells can be significantly improved by appropriated Co substitution. The prepared powder was identified as a single phase of nanocrystalline cubic spinel structure with a space group of Fd3m in which the lithium ions occupy the tetrahedral (8a) sites, and manganese and substituting Co metal ion reside at the octahedral (16d) sites. The cyclic voltammogram clearly indicates the reversibility of the cathode material and a two-step redox nature of the specimen into the $LiMn_2O_4$ spinel host matrix. The particle size of the products by CAM microwave-assisted sol–gel methods at the sub-micron level was confirmed by SEM analysis. The preparative process also yields a phase–pure product with controlled stoichiometry. Hence, $LiCo_xMn_{2-x}O_4$ powder obtained by CAM microwave-assisted sol–gel method could be used as an effective cathode material for Li ion batteries.

References

1. Tarascon JM, Wang E, Shokoohi FK (1991) J Electrochem Soc 138:2859
2. Bang HJ, Donepudi VS, Prakash J (2002) Electrochim Acta 48:443
3. Amine K, Tukamoto H, Yasuda H, Fujita Y (1996) J Electrochem Soc 143:1607
4. Fu YP, Su YH, Lin CH (2004) Solid State Ionics 166:137
5. Lu CH, Lin Y, Wang HC (2003) J Mater Sci Lett 22:615

6. Feng Q, Kanoh H, Miyai Y, Doi K (1995) Chem Mater 7:379
7. Thirunakaran R, Babu BR, Kalaiselvi N, Periasamy P, Kumar TP, Renganathan NG, Ragharan M, Muniyandi N (2001) Bull Mater Sci 24:51
8. Liu W, Kowal K, Farrington GC (1996) J Electrochem Soc 143:3590
9. Liu W, Farrington GC, Chaput F, Dunn B (1996) J Electrochem Soc 143:879
10. Zhecheva EN, Gorova MY, Stoyanova RK (1999) J Mater Chem 9:1559
11. Xia YY, Takeshige H, Noguchi H, Yoshio M (1995) J Power Sources 56:61
12. Hwang BJ, Santhanam R, Liu DG, Tsai YW (2001) J Power Sources 102:326
13. Berg H, Goransson K, Nolang B, Thomas JO (1999) J Mater Chem 9:2813
14. Rietveld HM (1969) J Appl Crystallogr 2:65
15. Amarilla JM, Martin de Vidales JL, Rojas RM (2000) 127:73
16. Shannon RD (1976) Acta Crystallogr A 32:751
17. Shen CH, Liu RS, Gundakaran R, Chen JM, Hung SM, Chen JS, Wang CM (2001) J Power Sources 102:21
18. Guohua L, Ikuta H, Uchida T, Wakihara M (1996) J Electrochem Soc 143:178
19. Chen CH, Liu RS, Gundakaran R, Shen MS (2001) J Chem Soc Dalton Trans 141:37
20. Xia Y, Yoshio M (1996) J Electrochem Soc 143:825
21. Saadounce I, Delmas J (1998) Solid State Chem 136:8
22. Wu XM, Li XH, Xiao ZB, Liu JB, Liu WB, Yan WB, Yan MB, Ma MY (2004) Mater Chem Phys 84:182